

Microsegregation during Solidification of an Al-Cu Binary Alloy at Largely Different Cooling Rates (0.01 to 20,000 K/s): Modeling and Experimental Study

GALINA KASPEROVICH, THOMAS VOLKMANN, LORENZ RATKE, and DIETER HERLACH

Microsegregation in the Al 4 wt pct Cu alloy was investigated experimentally in a large range of cooling rates from 0.01 to 20,000 K/s using different solidification techniques. The microstructure was modeled using two-dimensional (2-D) pseudo-front tracking (PFT) developed by Jacot and co-workers. The experimentally determined amount of nonequilibrium eutectics increases with the cooling rate in the range 0.01 to 3 K/s and then decreases in the range 20 to 20,000 K/s. The fraction of eutectic calculated from the 2-D PFT model shows not only the same tendency, but also agrees quantitatively very well with the experiments over the range of cooling rates. It can also be explained qualitatively how the observed in terms of coarsening of the secondary dendrite arms and the back diffusion in the way both depend on the local solidification time.

DOI: 10.1007/s11661-008-9505-6

© The Minerals, Metals & Materials Society and ASM International 2008

I. INTRODUCTION

SOLIDIFICATION of hypoeutectic alloys leads to microstructures in which the dendrites are embedded into a eutectic matrix. The amount of eutectic can be decomposed into equilibrium eutectic and nonequilibrium eutectic. Whereas equilibrium eutectic can be calculated by the lever rule, the nonequilibrium one depends on the local cooling history in a casting and on the microstructure evolution responding to it. If Scheil's model for microsegregation would apply, alloys would develop a eutectic fraction between the dendrites if the alloy's gross composition is below the maximum solubility of solute at the eutectic temperature (most wrought alloys). The origin is that Scheil's model does not take into account diffusion of the solute in the solid phase. Using equilibrium partitioning at the solid-liquid interface, this leads to an enrichment of solute in the liquid and a solute concentration in the solid phase, such that the solidification ends at the eutectic temperature with the appearance of eutectic. The difference between equilibrium solidification of such alloys (no eutectic) and nonequilibrium eutectic (NEE) in the Scheil case leads to the idea that back diffusion of the solute into the developing primary phase is responsible for an increase in NEE with decreasing solidification time. With increasing cooling rate or very small local solidification times, one would anticipate that Scheil's model could be applied and thus, the amount of NEE should increase from close to zero at small cooling rates to a maximum

value (calculated from Scheil's model) at large ones. Numerous studies, both experimental and theoretical, have been performed in the past to solve the issue of NEE beyond the simple ideas of equilibrium and Scheil solidification. The appearance of nonequilibrium in direct chill castings of wrought Al alloys can, for instance, lead to hot tearing.^[1]

However, the problem is not finally resolved. Table I gives some flavor of the controversy that exists in the literature regarding the effect of the cooling rate on the amount of nonequilibrium eutectic. Most investigations compiled in this table use binary Al-Cu alloys with a composition below the maximum solubility such that the eutectic appearing is of nonequilibrium character. Michael and Bever^[2] report that with increasing cooling rate, the amount of NEE increases as expected. The same tendency was observed by Taha *et al.*^[3] and Sarreal and Abbaschian,^[4] who found the amount of NEE to increase monotonically up to a cooling rate of 190 K/s, followed by a strongly reduced fraction of NEE at 1700 K/s (the value given for 37,000 K/s was taken from a sample that has a different gross composition). They interpret the "maximum" as a result of back diffusion, dendrite tip undercooling, and eutectic temperature depression. Novikov and Zolotarevskii^[5] report the same tendency as Sarreal and Abbaschian, namely, that there is a maximum in the amount of NEE; but the maximum value is achieved already at a cooling rate of 1 K/s instead of 190 K/s in Reference 4. Eskin and co-workers^[6] investigated several Al-Cu alloys cast into permanent molds made of various materials to achieve cooling rates ranging from 0.1 to 10 K/s. They also observed a maximum at the same cooling rate as Novikov and Zolotarevskii did. The same tendency as reported in Reference 6 was confirmed by Du and Eskin for the grain-refined Al 2.53 wt pct Cu alloy.^[7]

GALINA KASPEROVICH, THOMAS VOLKMANN, and LORENZ RATKE and DIETER HERLACH, Professors, are with the Institute of Materials Physics in Space, DLR, 51147 Cologne, Germany. Contact e-mail: galina.kasperovich@dlr.de

Manuscript submitted April 19, 2007.

Article published online March 27, 2008

Table I. Literature Data on the Effect of the Cooling Rate on the Amount of Nonequilibrium Eutectics

Alloy Composition (Wt Pct Cu)	Cooling Rate (K/s)	Variation in Amount of Nonequilibrium Eutectics with Cooling Rate	Comment	Reference
2, 3, 4, and 4.8	0.01, 0.8, 5, and 50	increase	mold casting	2
1, 3, and 4.5	1 to 38	increase	end-chill casting	3
2.8 and 4.9	0.1 to 37,000	increase to 190 K/s, then decrease	directional solidification	4
2 and 5	0.001 to 4	increase to 1 K/s, then decrease	quenched	5
0.98, 2.12, 3.24, and 4.3	0.1 to 10	increase to 1 K/s, then decrease	mold casting	6
2.53	0.1 to 20	increase to 1 K/s, then decrease	grain refined	7
5	1 and 3	increase	calculated, 1-D	7
2.53	0.8 and 16	increase	calculated, 1-D	7
2.53	0.8 and 16	decrease	calculated, 2-D	7

The table also lists a few theoretical investigations. As mentioned previously, back diffusion in the solid directly influences the prediction of the final eutectic fraction. The amount of solute transferred by back diffusion is proportional to the local concentration gradient at the periphery of a growing dendritic grain, the interfacial area, and the solidification time. Obviously, the longer the solidification time, the more solute can diffuse into the solid phase. Numerous models have been developed like those of Voller,^[8] Voller and Beckermann,^[9] Kobayashi,^[10] Wang and Beckermann,^[11] Ohnaka,^[12] and Nastac and Stefanescu,^[13] which essentially rest on a suitable treatment of the back diffusion, a description of the solute profile inside a secondary dendrite arm, *etc.* The main issue, as mentioned by Voller, always is the equilibrium partition coefficient k and the Fourier number being defined as $Fo = Dt_f/X^2$. In this relation, D is the solute diffusion coefficient in the solid primary phase, t_f the solidification time, and X a characteristic lengths scale, mostly taken as half the secondary dendrite arm spacing (SDAS) $X = \lambda_2/2$. All models predict an increasing amount of NEE with increasing cooling rate, and thus do not reproduce the experimental observations mentioned. New numerical models have been developed recently.

One-dimensional (1-D) and two-dimensional (2-D) pseudo-front tracking (PFT) modeling for an Al 2.53 wt pct Cu alloy has been performed by Du and Eskin^[7] for two cooling rates, 0.8 and 16 K/s. The 1-D PFT simulations for both slow and fast cooling cases have yielded higher values of the eutectic phase fraction than the experimental measurements. The 2-D PFT model predicts a decrease in the eutectic fraction with increasing cooling rate as observed in the experiments, however, the modeling was only performed for two cooling rates and thus makes the conclusion that it reflects the experiment somewhat optimistic.

Although the 1-D microsegregation PFT model by Jacot and Rappaz^[14] seems to predict the fraction of nonequilibrium phases, their average nature and the simplified grain morphology assumption make it impossible to describe how the interface dynamics and the spatial distribution of grain morphology affects the nonequilibrium phase formation. A new 2-D PFT model has been developed by Du and Jacot^[15] to combine a direct simulation of the primary phase formation based on a 1-D model and a mixture approach for the

description of the formation of secondary phases. The 2-D PFT describes the influence of back diffusion on the evolution of type, amount, and composition of the interdendritic phases, and thus the formation of non-equilibrium eutectic.

We therefore decided to perform a combined experimental and theoretical study on the amount of NEE using one alloy solidified over a very wide range of cooling rates. We employed for some experimental data points the 2-D PFT modeling of Jacot and co-workers provided by CALCOSOFT[®].^[16] Not only is the amount of NEE compared between experiment and model, but also the microstructure and microstructural features, such as SDAS, are also examined.

II. EXPERIMENTAL INVESTIGATION

To provide a large range of the cooling rates, four different techniques of solidification were used: (1) ARTEMIS facility (from 0.03 to 0.36 K/s); (2) aerogel, titan, steel, and copper mold casting (0.98, 22.3, 49.5, 117, and 232 K/s); (3) electromagnetic levitation (EML) (2.9 K/s); and (4) drop tube experiments (from 115 to 20,000 K/s). A binary Al 4 wt pct Cu master alloy was prepared in an electrical resistance furnace from 99.99 pct pure aluminum and 99.999 pct pure copper. No melt treatment or grain refinement was performed.

A. ARTEMIS Facility

Cylindrical samples (8-mm diameter, 120-mm length) with the composition Al 4 wt pct Cu were solidified directionally from the bottom to the top in the ARTEMIS facility at a constant temperature gradient of 3 K/mm under vacuum conditions. The solidification velocity was varied in the range of $v = 0.01$ to 0.12 mm/s.

The ARTEMIS furnace technology is described in References 17 through 19. Essential to the facility is the optical control of the processing due to the transparency of the aerogel^[20,21] and the flat isotherms in the samples due to the extremely low thermal conductivity of aerogels. With a line-NIR-camera (256 pixel), the sample surface in the area of the aerogel crucible (investigated zone is 63 mm) is observed during the experiments and the brightness along the cylinder axis is measured (for more details about the optical determination, see

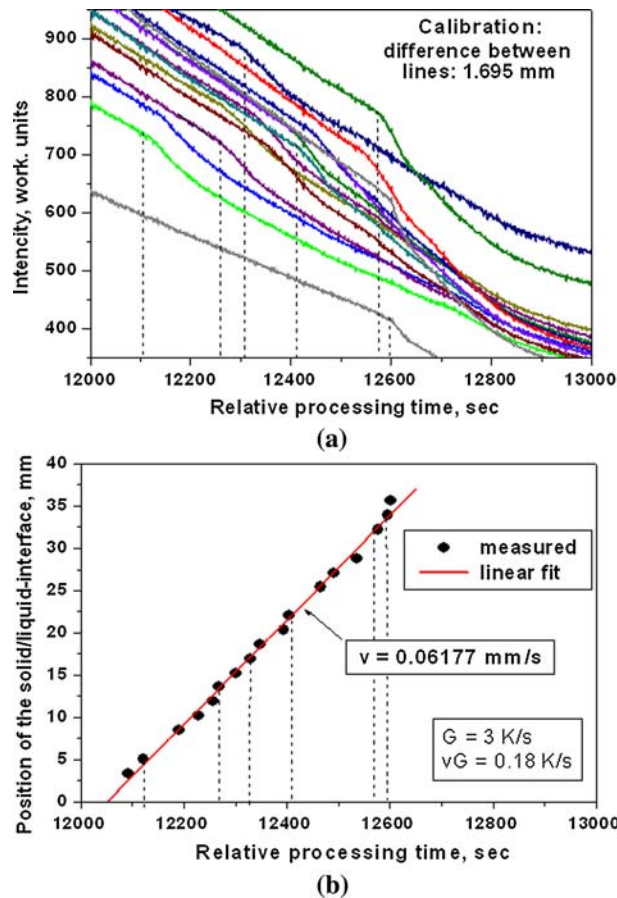


Fig. 1—Example of definition of solidification velocity in the ARTEMIS furnace technology: (a) measured intensity values for 17 selected, equidistant pixels vs experiment time; and (b) plot of the position/time values identified in (a), showing a linear curve revealing a constant solidification velocity of 0.06 mm/s.

References 22 and 23). Figure 1(a) shows an example of the intensity-time profiles measured in 17 different equidistant positions along the sample surface. The curves show a change in slope, which propagates through the pixel readings, *i.e.*, through the sample. This is attributed to the change in emissivity upon reaching the eutectic temperature (548 °C), where the sample fully solidifies. The position of the solid/liquid interface and the temperature gradient ahead of it can be extracted from intensity vs time profiles for each measurement, as shown in Figure 1(b). Six different cooling rates were examined: 0.03, 0.12, 0.18, 0.24, 0.30, and 0.36 K/s. The microstructure of the samples was evaluated on several sections being perpendicular to the growth direction and in line with it.

B. Mold Casting

A remelted batch of the master alloy was overheated to 750 °C and poured into different cylindrical molds made of various materials: aerogel, titan, steel, and copper. The cast cylinders had 60-mm height and 12-mm diameter. The variation in the cooling rate was due to the heat extraction capacity of the mold

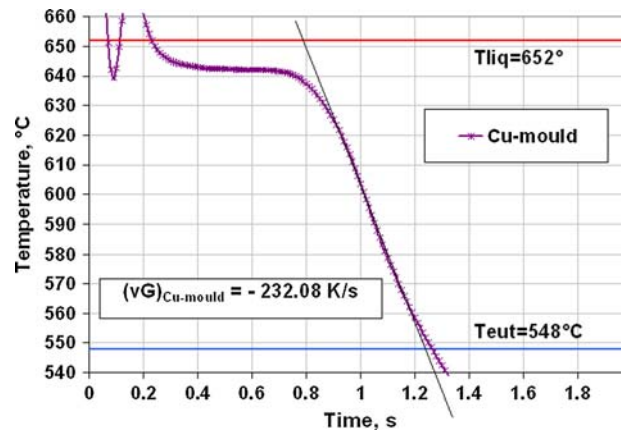


Fig. 2—Example of experimental cooling curve in mold casting experiments. Cooling rate is determined in the solidification interval as indicated by solid line. Sharp temperature increase at short times is due to latent heat release.

materials. The temperature at the middle of the alloy in 5-, 25-, and 45-mm length of the sample was recorded by a thin open-tip *K* thermocouple with a wire diameter of 0.15 mm. The cooling rate was calculated as the slope of the linear part of the cooling curve, as illustrated for the copper mold in Figure 2.

The cooling rates in this series of experiments were as follows: 0.98 and 22.3 for aerogel molds (with aerogel and steel bottom); and 49.5, 117, and 232 K/s for titanium, steel, and copper molds (with aerogel bottom), accordingly. The samples were cut in the horizontal plane as close as possible to the position of the thermocouple tip.

C. Electromagnetic Levitation and Drop Tube Facilities

Small pieces of the Al 4 wt pct Cu alloys were processed containerlessly by electromagnetic levitation (EML) and the drop-tube technique. The detailed descriptions of EML and drop tube experiment procedures are presented elsewhere.^[24–26]

Before levitation, an alloy sample of about 0.3 to 0.4 grams was placed onto a hollow quartz sample holder and positioned in the levitation coil of an EML facility.^[24] The levitation chamber was filled with highly purified helium gas (99.9999 pct) to a pressure of about 500 mbar. The alloy sample was then levitated and melted under this pressure. The sample was overheated to a temperature of 100 to 200 K above the liquidus temperature and subsequently cooled by blowing helium gas onto the sample surface. The sample temperature during solidification was measured using a two-color pyrometer with a relative accuracy of $\pm 5 \text{ K}$, and recorded using a transient recorder. The cooling rate in this experiment was calculated as the slope of the linear part of the cooling curve (as Figure 2 illustrates) and determined as 2.9 K/s.

For the drop tube experiments, an alloy of 1 gram was placed in a quartz tube with an orifice of 0.5 mm at the bottom. The quartz tube was positioned in a copper coil fixed at the top of an 8 m drop tube. The drop tube

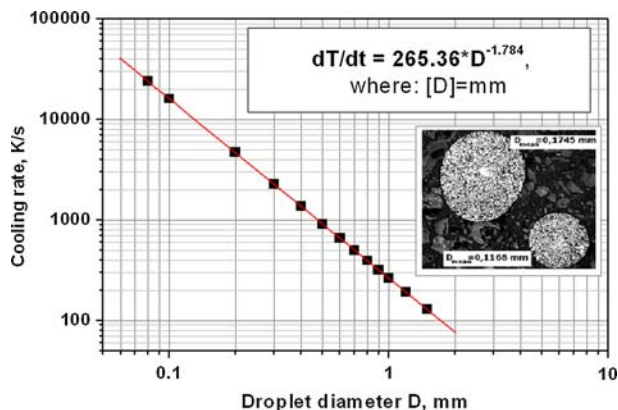


Fig. 3—Cooling rate as a function of the droplet diameter in drop tube technology calculated for Al 4 wt pct Cu alloy.

was filled with pure helium (99.999 pct purity) to a pressure of about 500 mbar. The alloy was inductively melted and heated to a temperature of 100 to 200 K above its liquidus temperature. The melt was ejected through the orifice by helium overpressure and atomized into droplets of diameters ranging from 0.1 to 2.0 mm. The droplets were solidified during their free fall in the drop tube. The solidified particles were collected at the bottom and sieved into several group sizes.

In this case, the cooling rate cannot be measured experimentally but has to be calculated from a suitable heat balance as a function of droplet size D ,^[25,27] taking into account the thermophysical properties of the Al 4 wt pct Cu alloy, the forced convection of the surrounding helium gas, radiation at the metal drop surface, and the latent heat release (Figure 3).

Together, 12 different droplets (\emptyset from 100 to 1500 μm) with cooling rates from 155 to 14,070 K/s were examined.

D. Microstructure Evaluation

All samples were ground, polished, etched with Kroll's reagent, and examined in an optical microscope. The dendrite arm spacing, volume fraction of the eutectic phase, and grain size were calculated using standard linear intercept methods both manually and using a quantitative image analysis program AnalySIS[®].^[28] Statistical analysis of the results was performed. For the composition measurements, the samples were examined with an LEO1530VP scanning electron microscope (SEM) under backscattering conditions. Elemental concentrations of the phase constituents and of the bulk samples were analyzed using an energy dispersive X-ray microanalyzer (EDX, INCA, Oxford, United Kingdom) fitted to the SEM.

III. THEORETICAL MODELING

The model combines a direct simulation of the primary phase formation based on the PFT method^[14] and a mixture approach for the description of the formation of secondary phases.^[15] The 2-D PFT model

Table II. Parameters in 2-D PFT Model

Alloy	Al 4 wt pct Cu (Al 1.71 at. pct Cu)
Phase diagram	linear binary phase diagram
Diffusion, m^2/s	$D_{\text{Cu}}^z = 0.65 \times 10^{-4} e^{-136,000/RT}$ $D'_{\text{Cu}} = 3 \times 10^{-9}$
Solid seed	
Number	10
Initial radius, μm	5
Position	random
Crystal orientation, θ_o	random
Last solidification stage, λ	0 (coupled)
Phase definition	LIQUID fcc-primary solid Al2Cu-secondary solid
Space and time	
Cell size, μm	1.25
Number of cells	400 × 400
Domain size (μm^2)	500 × 433
Coordinates	2d Cartesian
Solidification start, $^{\circ}\text{C}$	$T_{\text{liq}} = 648$
Solidification finish, $^{\circ}\text{C}$	$T_{\text{eut}} = 547.8$
Theoretical condition/ cooling rate	0.12 ÷ 14,070 K/s
Final time, s	835 ÷ 0.007
CPU time	from 1 ÷ 2 h to 1 to 2 months

takes into account both diffusion in the liquid and solid phases and curvature undercooling, which together determine the velocity of the solid-liquid interface. Therefore, this model can explicitly track how the grain morphology evolves. The curvature of the solid-liquid interface is calculated with the piecewise linear interface calculation technique.^[15,16] As soon as the liquid becomes undercooled for a secondary solid phase, the calculation enters a second stage in which the mixture approach is invoked and aimed at predicting the formation of secondary phases in the remaining interdendritic regions. In this approach, the interdendritic regions are considered as a mixture of liquid and solid phases. The model provides the evolution of the interdendritic mixture as solidification proceeds, taking into account the effects of back diffusion, which continuously modifies the composition and the volume of the interdendritic regions (more details can be found in References 14 and 15). Table II lists the parameters used for the calculations. Simulations of solidification experiments for some processed cooling rates ranging from 0.12 to 14,070 K/s were performed (Section II and Table III).

IV. RESULTS AND DISCUSSION

Figure 4 (on the left side) shows typical microstructures of the solidified Al 4 wt pct Cu alloy for some selected cooling rates. The structure changes from globular-dendritic in the range of slow cooling to needle-shaped dendritic at large cooling rates. The dendrite arms (α -Al, white area in the figures) are separated by θ -Al₂Cu (dark areas). In a larger magnification of the area around

Table III. Comparison of Experimental and Calculated Amount of Nonequilibrium Eutectics and Dendrite Arm Spacing λ_2 for Al 4 Wt Pct Cu Alloy

Solidification Technique	dT/dt (K/s)	SDAS (μm)			Amount of Eutectic (Wt Pct)		
		Experiment	PFT Calculation	Fourier Number	Experiment	PFT Calculation	
Artemis	$v = 0.01 \text{ mm/s}, G = 3 \text{ K/s}$	0.03	180.2	—	0.2005	1.36	—
	$v = 0.04 \text{ mm/s}, G = 3 \text{ K/s}$	0.12	116.7	112.0	0.1297	3.64	3.22
	$v = 0.06 \text{ mm/s}, G = 3 \text{ K/s}$	0.18	96.9	—	0.1134	3.85	—
	$v = 0.08 \text{ mm/s}, G = 3 \text{ K/s}$	0.24	86.1	86.7	0.1038	4.40	4.91
	$v = 0.10 \text{ mm/s}, G = 3 \text{ K/s}$	0.30	83.4	—	0.0964	5.12	—
	$v = 0.12 \text{ mm/s}, G = 3 \text{ K/s}$	0.36	76.9	75.3	0.0913	5.30	5.52
Mold casting	aerogel mold (aerogel bottom)	0.98	65.8	66.3	0.0663	5.78	6.72
	aerogel mold (steel bottom)	22.3	23.5	19.5	0.0245	4.56	4.41
	titan mold (aerogel bottom)	49.5	16.2	15.5	0.0190	3.25	3.71
	steel mold (aerogel bottom)	117	13.0	12.6	0.0145	1.68	1.88
	copper mold (aerogel bottom)	232	9.81	9.44	0.0117	1.22	1.44
Levitation		2.9	38.5	38.5	0.0471	6.32	7.48
Drop tube	drop \varnothing : 1351.3 μm	155	10.5	11.0	0.0135	1.79	1.91
	drop \varnothing : 916.6 μm	310	8.28	8.46	0.0107	1.04	1.17
	drop \varnothing : 794.7 μm	400	7.67	8.20	0.0098	0.98	1.11
	drop \varnothing : 590.4 μm	680	6.43	6.55	0.0083	0.96	1.11
	drop \varnothing : 480.0 μm	980	5.82	5.44	0.0074	0.96	1.06
	drop \varnothing : 264.6 μm	2850	3.84	4.06	0.0053	0.68	0.79
	drop \varnothing : 248.0 μm	3200	3.90	3.84	0.0051	0.59	0.69
	drop \varnothing : 209.2 μm	4300	3.35	3.62	0.0048	0.58	0.66
	drop \varnothing : 174.5 μm	6000	3.31	3.22	0.0047	0.56	0.80
	drop \varnothing : 137.8 μm	9100	2.88	3.12	0.0044	0.52	0.56
	drop \varnothing : 116.8 μm	12,200	3.06	2.68	0.0043	0.48	0.50
	drop \varnothing : 108 μm	14,070	2.53	2.34	0.0041	0.42	0.43

the θ phase (Figure 5), one can observe different gray scales mirroring the varying contents of the solute in the primary α phase. The image size in Figure 5 is $570 \times 427 \mu\text{m}$ for all cuts.

The right side of Figure 4 presents Cu concentration contours obtained from the 2-D PFT calculations at the last stage of solidification. The left and right panels in Figure 4 match in the cooling rates. Different gray shades indicate different Cu concentration (scale on the left, where the dark areas correspond to the maximum Cu concentration). The domain size is $500 \times 433 \mu\text{m}$.

Figure 5 shows a comparison of the measured and calculated solute concentration for a cooling rate of 0.12 K/s. The PFT predictions of the Cu concentration shown in Figure 5(b) agree well with experimental measurements (Figure 5(a)), giving trust to the predictive power of the model. For example, the experimental Cu concentration in the eutectic area is 17.57 at. pct and the corresponding simulation value of the PFT calculation 16.8 at. pct Cu. Following the evolution of the Cu distribution during the primary and secondary phase formation as a function of time, one can predict the microsegregation processes in different areas. It is possible to observe, for example, that the first portion of the α -Al phase has smaller Cu concentration (about 0.5 at. pct), then the concentration increases and finally reaches 0.97 at. pct (line 3 in Figure 5(b)). The corresponding experimental value is 0.85 at. pct Cu.

The secondary dendrite arm spacing (SDAS, I_2) is an important parameter to qualify back diffusion through

the Fourier number as explained previously. We therefore measured the SDAS and the grain size both in the experiments and in the simulations using the same metallographic technique. An example of SDAS definition and evaluation with the image analysis software is shown in Figure 6. In the experiment (Figure 6(a)), we obtain an average λ_2 value of 9.81 μm for the parameters given in the figure caption. In the PFT simulation, the mean intercept method was applied in order to determine the typical diffusion distance λ_2 , which corresponds to the secondary arm spacing in the dendritic structure and the grain size in the globular structure as shown in Figure 6(b). The value of λ_2 determined in this way as 9.44 μm corresponds well to the experimental one. The average values of the experimental spacings for all cooling rates, which had a maximum deviation of ± 10 pct, and simulated values are summarized in Table III. The simulated dendrite arm spacings are also in good accordance with the measured experimental values and could well be described over the whole range of cooling rates (0.01 to 20,000 K/s) with a following approximation (Figure 7):

$$\lambda_2 = 54.50 (dT/dt)^{-0.328} \quad [1]$$

The error estimate for the amplitude in Eq. [1] is ± 0.01 and ± 0.003 for the exponent. The relative differences of the DAS between the experiments and the simulation runs were not larger than 8 pct. Therefore, one can conclude that the 2-D PFT simulations

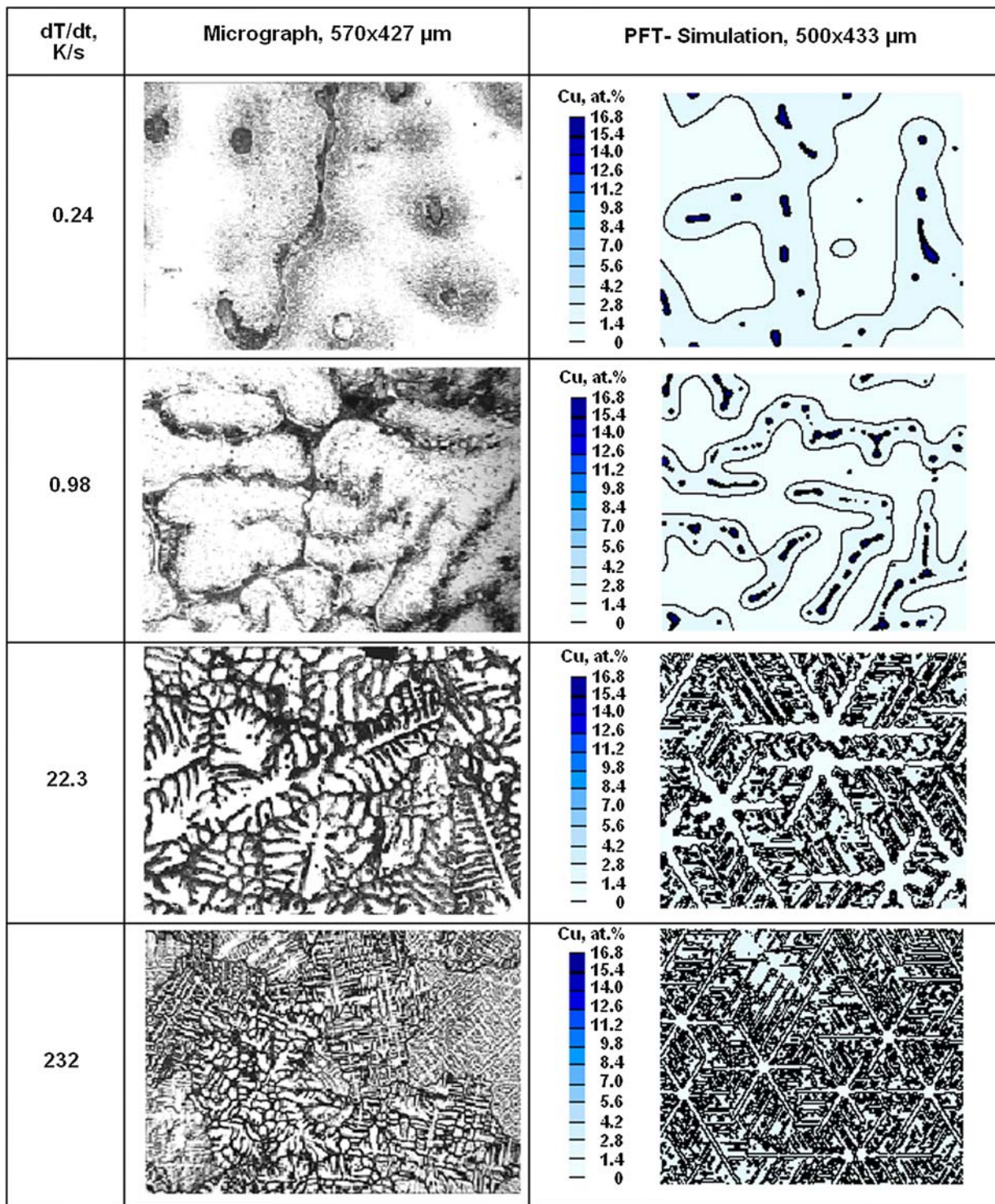


Fig. 4—Experimental (left) and modeled (right) microstructures for some slow (0.24 and 0.98 K/s) and some rapid (22.3 and 232 K/s) cooling rates. Experimental micrographs are received from an optical microscope; samples were etched with Kroll's reagent. Image size is $570 \times 427 \mu\text{m}$ for experimental and $500 \times 433 \mu\text{m}$ for modeled microstructures.

reproduce the observed microstructure, and therefore can be used to investigate the influence of the cooling rate on the amount of NEE.

The experimentally determined dependence of the NEE fraction on the cooling rate is shown in Figure 8 and compared to values determined by the 2-D PFT simula-

tions. Although there are some differences between the experimental data points and the ones calculated with the PFT model, both exhibit the same tendencies: the volume fraction of NEE increases with the cooling rate in the range up to approximately 3 K/s, and then decreases in the range of cooling rates from 20 to 20,000 K/s.

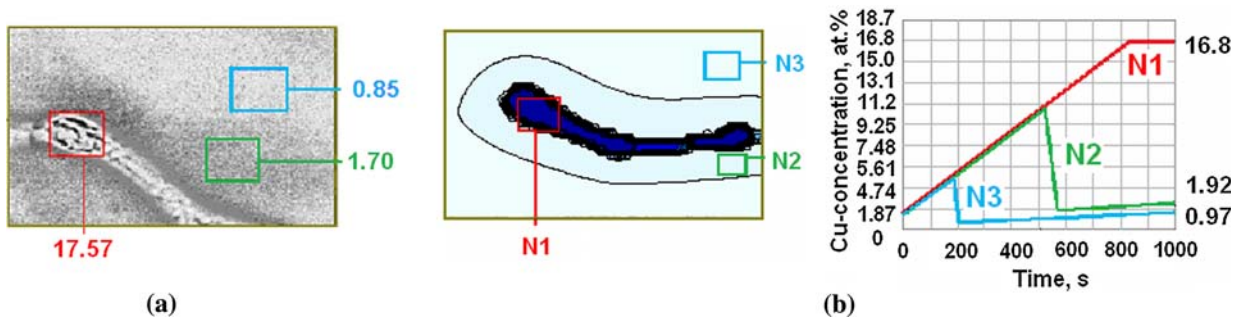


Fig. 5—Microstructure and Cu concentration of a non-grain-refined Al 4 wt pct Cu alloy obtained after solidification at 0.12 K/s: (a) measured and (b) simulated. Figure designations are Cu concentration (in atomic percent) in the different areas in image (a) and the evolution of Cu concentration with time (the diagram to the right in (b)). Image size is $10 \times 6 \mu\text{m}$ for (a) and $10 \times 6.5 \mu\text{m}$ for (b). Image (a) is received from raster electron microscopy with differential contrast enhancement filter.

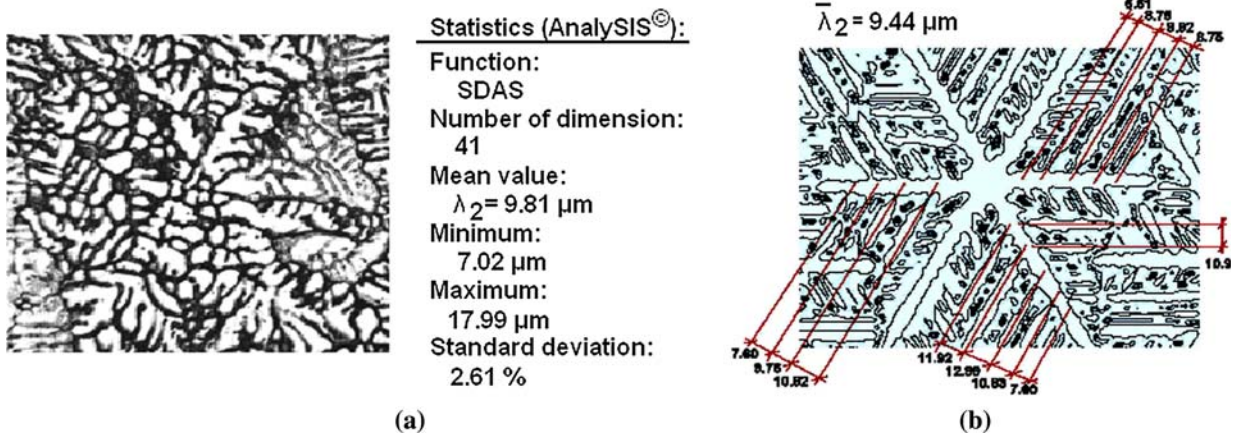


Fig. 6—Microstructure and SDAS definition of a non-grain-refined Al 4 wt pct Cu alloy obtained after solidification at 232 K/s: (a) using the quantitative image analysis program AnalySIS and (b) in the PFT simulation. Image size is $190 \times 164 \mu\text{m}$ for (a) and $192 \times 156 \mu\text{m}$ for (b). Image (a) is obtained from an optical microscope; sample was etched with Kroll's reagent. Experimentally determined mean λ_2 in accord to statistics in the AnalySIS dimensions is $9.81 \mu\text{m}$ (a) and corresponds to mean quantity λ_2 from simulation $9.44 \mu\text{m}$ (b).

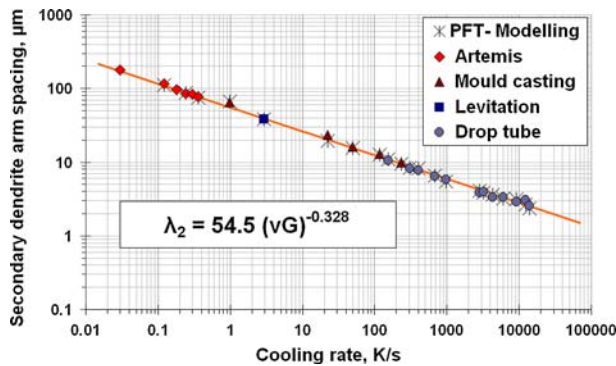


Fig. 7—SDAS as function of cooling rate for Al 4 wt pct Cu alloy for a large range of the cooling rates.

In the different microsegregation and coarsening models mentioned previously,^[8–13] the amount of NEE depends mainly on the Fourier number, Fo. The Fourier number was calculated using the diffusion coefficient of Cu in α -Al as given in Table II, the SDAS using Eq. [1] and the local solidification time was taken from the PFT modeling. The result is shown in Table III. The volume

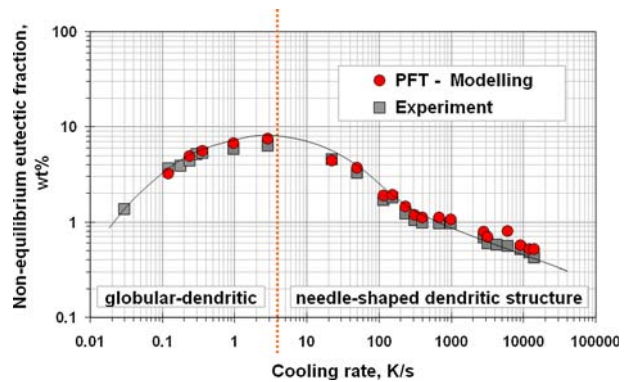


Fig. 8—Effect of cooling rate on the amount of nonequilibrium eutectics in binary Al 4 wt pct Cu alloy. Tendency changes from increase in the range of slow cooling ($dT/dt < 3 \text{ K/s}$) to decrease by fast cooling rates ($dT/dt = 20$ to $20,000 \text{ K/s}$). It should be observed that dendritic structure has globular-dendritic form by slow cooling (Fig. 4, cooling rates: 0.24 and 0.98 K/s) and needle-shaped structure by fast cooling (Fig. 4, cooling rates: 22.3 and 232 K/s).

fraction of NEE increases in the range of Fourier numbers up to approximately 0.04 (fast cooling) and decreases when the Fourier is larger than 0.04 (slow cooling).

A comparison of our results with those in the literature mentioned previously shows that we can confirm that there is a maximum amount of NEE depending on cooling rate or Fourier number.^[4,6] In contrast to the recent work of Du and Eskin,^[7] we have a large range of cooling rates both in experiments and simulations. The result is in contradiction to theories based solely on Fourier number and partition coefficient. The models mentioned in Section I^[8-13] predict, to our understanding, no maximum but a continuous increase with cooling rate (which is a decreasing Fourier number). Although the PFT model reflects the data so well, we think that an understanding in terms of operating physical mechanisms would be nice. The maximum is a result of two opposing effects. As shown in Figure 7, the SDAS decreases with increasing cooling rate and it is especially obvious that the microstructure exhibits much more interfacial area between the primary phase and the interdendritic region. Figure 9 shows a result of the PFT modeling, namely the volumetric back diffusion rate, which is the volume of Cu that diffuses per second into the primary phase through the phase boundary. This volumetric rate increases with increasing cooling rate, approximately like $(dT/dt)^{4/5}$. The volumetric flux is a complicated function of the flux gradient at the interface, the surface area of the dendrites, and their local thickness. We assume that the following consideration is valid: the larger the amount of volumetric back diffusion, the smaller the amount of solute atoms left in the interdendritic liquid that can form nonequilibrium eutectic. On the other hand, the larger the SDAS, the larger the diffusion distances in the melt, and thus the larger the amount of solute left in the melt to form the eutectic phase. The dependence of both expressions on cooling rate reflects in a certain way the reaction of NEE on cooling rate. Their joint action would then lead to a maximum of nonequilibrium eutectic. Much better than these simple considerations is the 2-D PFT model developed by Jacot and co-workers,^[14,15] which has been applied here for the calculations. It describes well the microstructure evolution, the back diffusion, and the diffusion in the liquid and solid phase such that the type, amount, and composition of the interdendritic phases and especially the amount of NEE are very well reproduced.

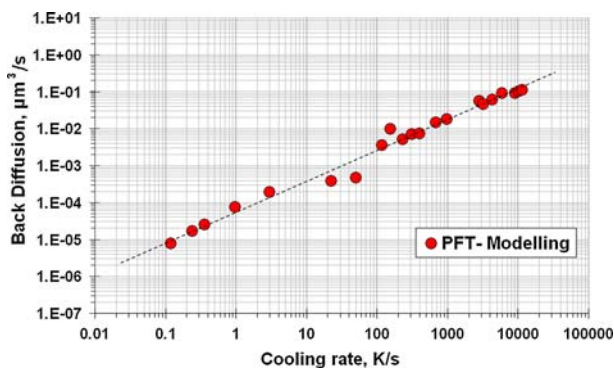


Fig. 9—Back diffusion as function of cooling rate for Al 4 wt pct Cu alloy.

Finally, we would like to consider if fluid flow could have influenced the solute redistribution and thus the amount of NEE. If convections would have affected the solidification in our experiments, we could have observed, for instance, macrosegregation^[29,30] and a change in the kinetics of SDAS from a cube root law to a square root dependence on cooling rate.^[31,32] Independent of the solidification technique used all SDAS values measured are close to the expected cube root law as shown in Figure 7, with no perceptible hint of a deviation from it in any interval of the cooling rate. One would, however, not expect a deviation from the cube root behavior over the whole range of cooling rates. Flow-induced faster dendrite coarsening needs flow velocities larger than the solidification velocity.^[31,32] Thus, we would only expect a deviation at low cooling rates. The data show no hint of a deviation toward a square root instead of a cube root anywhere. Therefore, we conclude from the SDAS measurements that large scale flow was not relevant in our experiments.

This conclusion can be further substantiated by considering possible flow sources leading to possible macrosegregation. The slow cooling rates were generally achieved by using directional solidification within the ARTEMIS facility. In this facility, we know from a large number of experiments with other types of Al alloys (AlSi base) and a few experiments performed under microgravity conditions, that there is no fluid flow in the lower half of the samples^[33,34] where we made our evaluation. In addition in Al-Cu alloys, the solute partitioning should lead to a stable density layering, and thus no thermal or solutal convection is initiated on a coarse scale. There might be a thermosolutal convection on the scale of the dendrites due to the fact that the isoconcentration lines somehow mirror the contours of the dendrites, and thus they are partly inclined to the gravity vector leading to small scaled convection rolls. Their velocity will generally be small due to the fact that at the interface between the dendrites and the interdendritic liquid, a no-slip boundary condition holds. In as much as the fraction solid increases, this type of flow would be damped. In the drop tube experiments, the microstructures of two samples shown in Figure 3 clearly are very homogeneous with no hints for a macrosegregation. In the mold casting with the intermediate cooling rates, the solidification is radial, and thus the columnar dendrites appear close to the mold wall and grow toward the center, where an equiaxed dendritic structure is observed. The columnar dendrites are approximately perpendicular to the gravity vector, and thus natural convection could be expected. The alloy composition in the center, where we measured the SDAS and the amount of NEE, was exactly the nominal composition in all cases as determined from EDX measurements in the SEM, and also from image analysis on SEM pictures. Thus, we have no sign of macrosegregation in all mold cast samples. We therefore conclude that under the given circumstances in our experiments, the microstructure was not affected by possible fluid flow in a way that a comparison with the fluid flow free simulations of the PFT model would not be allowed or leading to false conclusions.

V. CONCLUSIONS

Microsegregation in the Al 4 wt pct Cu alloy was investigated experimentally in a large range of cooling rates from 0.01 to 20,000 K/s using different solidification techniques. The microstructure was modeled using 2-D PFT developed by Jacot and co-workers.^[14,15] The experimentally determined amount of nonequilibrium eutectics increases with the cooling rate in the range 0.01 to 3 K/s and then decreases in the range 20 to 20,000 K/s. The fraction of eutectic calculated from the 2-D PFT model shows the same tendency. The experimentally observed dependence of the fraction of nonequilibrium eutectics on the cooling rate can be qualitatively explained in terms of coarsening of the secondary dendrite arms and the back diffusion, as both depend on the local solidification time.

ACKNOWLEDGMENTS

This work was performed within the framework of the research program of Virtual Institute for Virtual MATerials design (VIVIMAT). The authors thank Dr. M. Kolbe, for the fruitful discussion about the definition of cooling rate in the drop tube facility and for helping in the microstructure analysis with SEM, and Mr. F. Schmidt-Hohagen, whose temperature measurements in the molds gave the background for definition of the cooling rate by the mold casting experiments. The authors are grateful to Dr. A. Jacot for numerous and fruitful explanations regarding the PFT model and its functioning as implemented in a CALCOSOFT code.

REFERENCES

1. M. Rappaz and W.J. Boettinger: *Acta Mater.*, 1999, vol. 47 (11), pp. 3205–19.
2. A.B. Michael and M.B. Bever: *Trans. AIME J. Met.*, 1954, vol. 202, pp. 47–56.
3. M.A. Taha, N.A. El-Mhallawy, and R.M. Hamouda: *Mater. Des.*, 2002, vol. 23, pp. 195–200.
4. J.A. Sarreal and G.J. Abbaschian: *Metall. Trans. A*, 1986, vol. 17A, pp. 2063–73.
5. I.I. Novikov and V.S. Zolotarevskii: *Dendritnaja Likvatsiya v Splyavakh (Dendritic Solidification in Alloys)*, Nauka, Moscow, 1966.
6. D. Eskin, Q. Du, D. Ruvalcaba, and L. Katgerman: *Mater. Sci. Eng.*, 2005, vol. A405, pp. 1–10.
7. Q. Du, D.G. Eskin, and A. Jacot: *Acta Mater.*, 2007, vol. 55 (5), pp. 1523–32.
8. V.R. Voller: *J. Cryst. Growth*, 2001, vol. 226, pp. 562–68.
9. V.R. Voller and C. Beckermann: *Metall. Mater. Trans. A*, 1999, vol. 30A, pp. 2183–89.
10. S. Kobayashi: *J. Cryst. Growth*, 1988, vol. 88, p. 87.
11. C.Y. Wang and C. Beckermann: *Mater. Sci. Eng.*, 1993, vol. A171, pp. 199–211.
12. I. Ohnaka: *Trans. ISIJ*, 1986, vol. 26, p. 1045.
13. L. Nastac and D.M. Stefanescu: *Metall. Trans. A*, 1993, vol. 24A, p. 2107.
14. A. Jacot and M. Rappaz: *Acta Mater.*, 2002, vol. 50, pp. 1909–26.
15. Q. Du and A. Jacot: *Acta Mater.*, 2005, vol. 53, pp. 3479–93.
16. CALCOSOFT, User Manual, Calcom ESI and Swiss Federal Institute of Technology, Lausanne, Switzerland, 2004.
17. J. Alkemper, S. Sous, C. Stöcker, and L. Ratke: *J. Cryst. Growth*, 1998, vol. 191, pp. 252–60.
18. S. Sous and L. Ratke: *Z. Metallkd.*, 2005, vol. 96 (4), pp. 362–69.
19. J. Alkemper, L. Ratke, and S. Sous: *Proc. 4th Decennial Conf. on Solidification Processing*, J. Beech and H. Jones, eds., Sheffield University, Sheffield, United Kingdom, 1997, pp. 463–67.
20. J. Fricke: *J. Non-Cryst. Solids*, 1992, vol. 145, pp. 1–259.
21. P.H. Tewari, A.J. Hunt, J.G. Lieber, K. Lufftus, and J. Fricke: *Aerogels*, Proc. Physics 6, Springer-Verlag, Berlin, 1986.
22. S. Steinbach and L. Ratke: *Scripta Mater.*, 2004, vol. 50, pp. 1135–38.
23. S. Steinbach and L. Ratke: *Mater. Sci. Eng.*, 2005, vols. A 413–A414, pp. 200–04.
24. D.M. Herlach, R.F. Cochrane, I. Egry, and H.J. Fecht: *Int. Mater. Rev.*, 1993, vol. 38 (6), pp. 273–347.
25. F. Gillesen: *Forschungsbericht DFVLR*, DLR-FB, Köln, 1989, pp. 89–32.
26. S. Reutzel, T. Volkmann, J. Gao, J. Strohmenger, and D.M. Herlach: in *Solidification and Crystallization*, D.M. Herlach, ed., Wiley-VCH, Weinheim, Germany, 2004, pp. 239–49.
27. P.S. Grant, B. Cantor, and L. Katgerman: *Acta Metall. Mater.*, 1993, vol. 41, pp. 3097–3108.
28. AnalySIS©, Soft Imaging System GmbH, 1986–2002.
29. R. Mehrabian and M.C. Flemings: *Metall. Trans.*, 1970, vol. 1, pp. 455–64.
30. C. Beckermann: *Int. Mater. Rev.*, 2002, vol. 47 (5), pp. 243–61.
31. L. Ratke and S. Steinbach: *Solidification Processing*, Proc. 5th Decennial Int. Conf. on Solidification Processing, Howard Jones, ed., University of Sheffield, Sheffield, United Kingdom, 2007, pp. 14–17.
32. H.-J. Diepers, C. Beckermann, and I. Steinbach: *Acta Mater.*, 1999, vol. 47, pp. 3663–78.
33. M. Hainke: Ph.D. Thesis, University of Erlangen–Nuremberg, Germany, 2004.
34. S. Steinbach and L. Ratke: *Proc. 18th Eur. Sounding Rocket & Balloon Programme Symp.*, W. Herfs and A. Wilson, eds., Visby, Sweden, 2007, ESA-SP 647, Special Publications No 647, ESA Publications Division, Noordwijk, The Netherlands, pp. 373–78.